STRUCTURAL CONTROLS ON FLUID MIGRATION AND SEISMIC VARIABILITY IN NORTHERN OKLAHOMA

A Thesis

Presented to the Faculty of the Graduate School

of Cornell University

In Partial Fulfillment of the Requirements for the Degree of

Master of Science

by

Catherine Elizabeth Lambert

August 2017

ABSTRACT

Abundant seismicity in north-central Oklahoma occurs throughout a region containing both mature, high-offset faults, and zones of sparse, short faults. This study uses a new seismicity catalog from 2015-2016 to show that earthquakes are, counterintuitively, most abundant throughout the regions of sparsely-mapped faults, occurring predominantly in basement away from mapped structures. Earthquakes are not detected on large, mapped faults bounding the Nemaha uplift, and earthquakes within the bounds of the uplift occur in rare and discrete clusters near wells. In addition to a catalog of precise earthquake locations, we calculate seismicity migration rates and focal mechanisms. We interpret the variation in seismicity across the uplift as the result of variations in fault density, fracturing, and resulting permeability structure. We suggest that the active seismicity along the edges of the uplift combined with the paucity of earthquakes on and between the large mapped faults indicates that the large faults are likely low permeability baffles for across-fault flow, impeding fluid migration into the uplift. Fault baffles would buffer the interior of the uplift from the regional fluid pressurization thought to cause the temporally expanding zone of seismicity. Within the uplift, in the zone of low seismicity, enhanced fracturing, faulting, and related basement alteration may create efficient fluid pathways that facilitate pressure diffusion away from local wells and modulate the seismicity rate.

BIOGRAPHICAL SKETCH

Catherine Lambert is a Finger Lakes native, born and raised in Elmira, NY. She attended the University of Rochester for her undergraduate degrees, earning a Bachelor of Science in Geological Science and a Bachelor of Arts in English in 2014. After completing her Masters in Geological Science in the Department of Earth and Atmospheric Sciences, Catherine will be pursuing a PhD in the Department of Communication at Cornell, studying risk and science communication.

ACKNOWLEDGMENTS

I would like to thank my advisor Katie Keranen and the members of the Keranen/Abers lab, particularly those who assisted with fieldwork in Oklahoma. Thank you to Stephanie Nale, Dana Peterson, Kayla Crosbie, and Nate Stevens for their support and friendship. I would also like to offer special thanks to the gracious Oklahomans who hosted our seismic stations and occasionally hauled me and various vehicles out of the mud. As always, thank you to my parents and siblings for their love and support.

This work was supported through grant NSF GRFP DGE-1650441 and NSF EAR-1554846 from the National Science Foundation, as well as generous support from the Cornell Earth Energy Institute.

TABLE OF CONTENTS

LIST OF FIGURES

LIST OF TABLES

LIST OF ABBREVIATIONS

OCC: Oklahoma Corporation Commission

OSU: Oklahoma State University

INTRODUCTION

Seismicity in north-central Oklahoma

In the last ten years, there has been a rapid rise in seismicity in Oklahoma, with the rate of M3 earthquakes increasing from an average of 1-2 M3 per year to more than 900 in 2015. During this time period, the region hosting seismicity increased from ~4,000 square km in 2010, to ~19,000 square km by 2015 *[ANSS]*. Notable earthquake sequences within Oklahoma include mainshocks and aftershocks of the 2011 Prague M5.7 earthquake and the 2016 Pawnee M5.8 earthquake, the largest in the state's history. Earthquakes occur predominantly from 2 to 6 km depth, the majority rupturing faults in crystalline basement. The rapid uptick in seismicity is considered to be the result of fluid injection, primarily during wastewater disposal *[e.g., Ellsworth, 2013; Keranen et al., 2014; Weingarten et al., 2015]*.

Since 2013, earthquakes have occurred primarily within a broad region in central and north-central Oklahoma, with two discrete, expanding centers of seismicity separated from each other by the Nemaha uplift (Figure 1). These expanding zones are thought to represent widespread subsurface pressurization, including at distances of over 20 km from wells *[e.g., Keranen et al., 2014; Yeck et al., 2016]*. As the zones of active seismicity have expanded (Figure 1, 7a), they have approached the large faults of the Nemaha uplift; however, the uplift itself has continued to exhibit relatively low levels of seismicity.

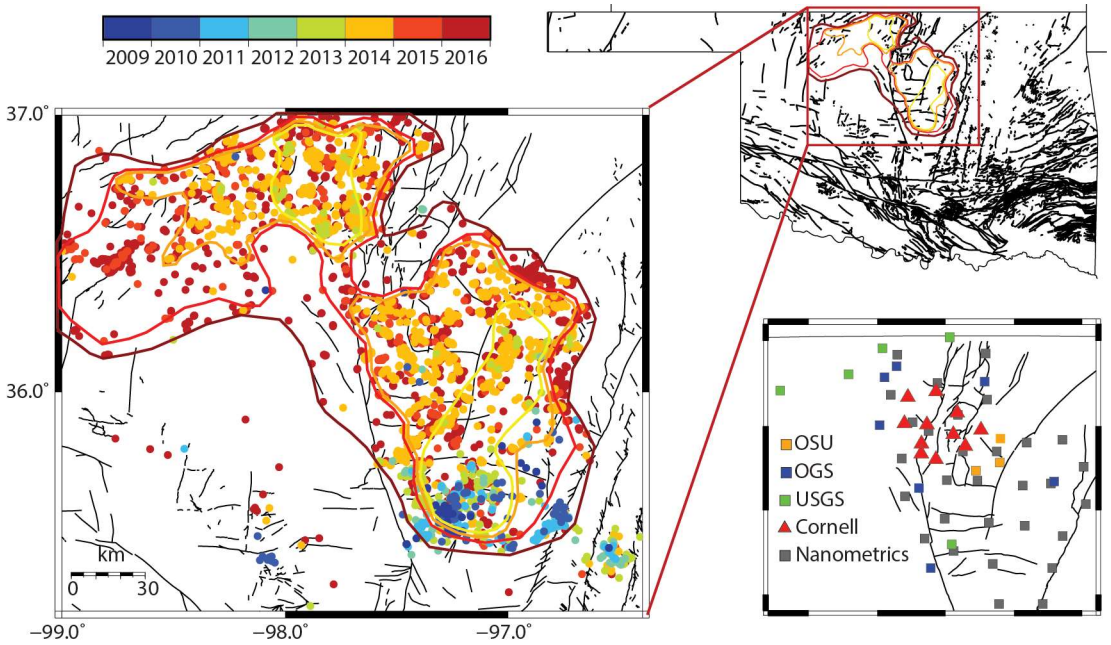

Figure 1. Seismicity surrounding the Nemaha Uplift in north-central Oklahoma. Contour lines show regions of active seismicity in 2013-2016. Lower right: station locations. Nanometrics stations were not used in the main catalog but were used in a catalog spanning 2013-2015.

Data source: ANSS Earthquake Catalog, USGS. Fault map from Marsh and Holland *[2016]*

In this paper, we investigate how the large faults of the Nemaha uplift interact with ongoing fluid migration and regional pressurization. The relative lack of seismicity within the Nemaha uplift bracketed by the expanding zones of seismicity on either side provides an opportunity to study variability in seismic response to regional fluid pressurization. We use a newly developed catalog of seismicity from a temporary seismic network within and surrounding the Nemaha uplift, combined with data from seismometers in permanent networks, to characterize the seismic response of the fault zone and the interactions between the large faults and migrating fluid pressure. By using a local catalog with enhanced recording of low magnitude earthquakes, we identify active faults in the basement that are hosting seismicity within and around the Nemaha uplift. Characterizing the variability of the seismic response across the uplift illuminates the role of the structural setting in mediating regional pressurization from wastewater injection, offering insight into how the Nemaha uplift, a structural feature that includes large, high-length faults that pose a potential hazard for central Oklahoma, may control regional patterns of seismicity.

Geology of the Nemaha uplift

The Nemaha uplift is a transpressional structural feature in Nebraska, Kansas, and northern Oklahoma, characterized by Precambrian basement uplifted during the Pennsylvanian period *[Dolton & Finn, 1989; McBee, 2003]*. The uplift trends NW-SE in northern Oklahoma and N-S in central Oklahoma, where it narrows to a single fault *[e.g., Marsh & Holland, 2016; McBee, 2003]*. The Nemaha uplift is a complex fault structure composed of a series of large, near-vertical, sub-parallel faults bordering

uplifted basement blocks *[Gay, S. Parker, 2003a, 2003b]*. Individual mapped fault segments reach over 100 km in length, with displacement in northern Oklahoma ranging from < 30 to ~480 m. The maximum uplift in our study area occurs on the eastern border fault of the uplift, reaching maximum offset at the Garber Field. Orthogonal fracture and joint patterns trend at 75° and at 155° *[Liu, Crampin, & Queen, 1991]*; predominant fault strike direction is 30°. The Garber Field is a pop-up block with an associated graben, and provides evidence for right-lateral strike slip movement along with the vertical offset.

The Nemaha Uplift is situated on the northeastern shelf of the Anadarko Basin, a sedimentary basin found in Oklahoma and Texas with multiple oil and gas bearing formations. On the west side of the uplift, formations dip gently to the west at <1 degrees *[Dana, 1955; McBee, 2003]*. These formations include the Arbuckle Group, a sedimentary unit atop basement which is dominantly limestone and dolomite. Though the Arbuckle Group is an oil-bearing unit in regions, the high permeability and porosity of the Arbuckle became a dominant target for wastewater disposal *[Morgan & Murray, 2015]*. Above the Arbuckle Group lie the Wilcox Sand, Simpson Sand, Viola Lime, Hunton Lime, Woodford Shale, and Mississippi Lime formations, where oil and gas production are currently ongoing *[Cary, 1955; OCC 2017]*. The Precambrian basement also dips gently to the west at ~1 degrees in our study area *[McBee, 2003]*, with depth to basement in and around the Nemaha Uplift ranging from 1-2 km *[McBee, 2003; Shah & Keller, 2017]*.

Wastewater Disposal

In Oklahoma, wastewater co-produced during oil and gas production is primarily disposed of via injection into deep disposal wells. The primary target reservoir for disposal wells is the Arbuckle Limestone, a Cambrian/Ordovician unit of primarily carbonates, including zones of high permeability developed by fracturing, erosion, and karst formation following early Ordovician subaerial exposure *[Morgan & Murray, 2015]*. Throughout the state, injected volumes increased rapidly beginning between 2004 and 2008; in our study area of north-central Oklahoma in Grant, Garfield, Noble, and Kay Counties, injection has been ongoing since the 1950s, but monthly rates increased from an average of ~5000 barrels (bbl) per month before 2004 to ~80,000 bbl per month during 2004-2015 *[OCC]*. From 2011 to 2015, average monthly rates of fluid injection ranged from <50,000 bbl to ~850,000 bbl per month at individual wells *[OCC]*. Areas of densest injection, with a combined >1 million barrels per month, occur near the central uplift and to the northwest of the uplift (Figure 2).

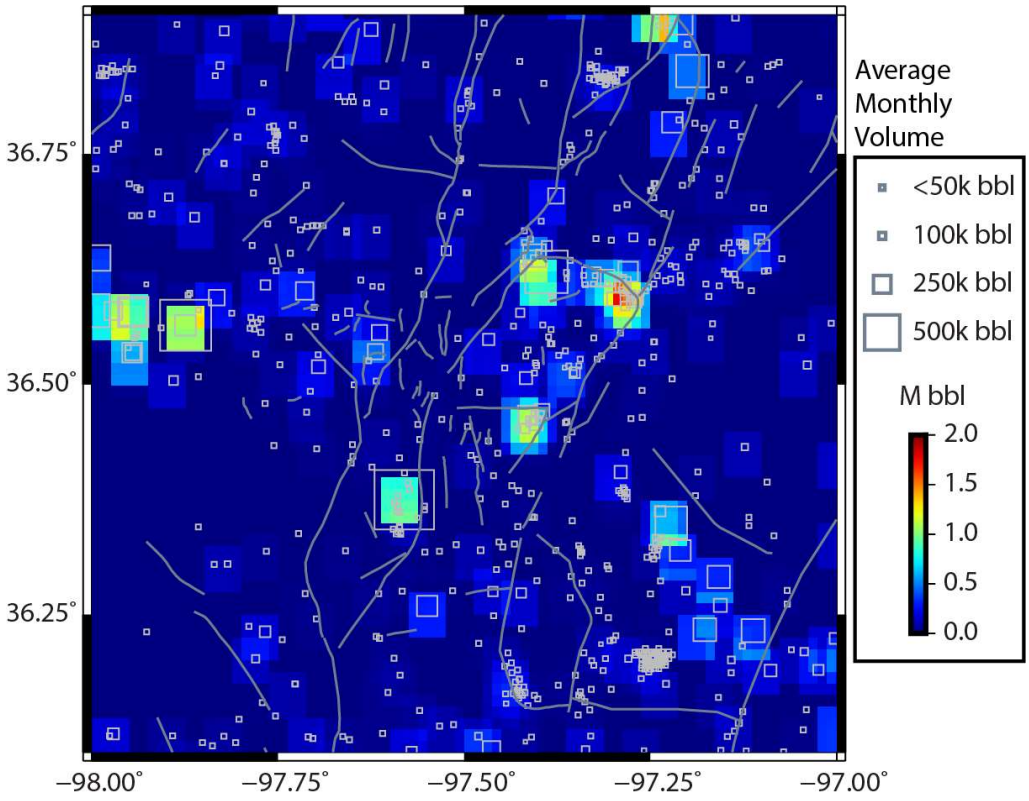

Figure 2. Average monthly volumes of wastewater injection in Arbuckle wells in study area, 2011-2015.

Data source: Oklahoma Corporation Commission (OCC) UIC injection volumes, 2011-2015. Fault map from Marsh and Holland *[2016]*

METHODS

In April 2015, we deployed ten Cornell University seismometers across the Nemaha Uplift and the bordering regions exhibiting elevated seismicity to the southeast and northwest. Our array spanned ~50 km, with a nominal station spacing of 15 km (Figure 1, inset). The three-component Trillium Compact seismometers sampled at 250 samples per second. These data are complemented by data recorded at 19 seismic stations operated by the USGS, OGS, and OSU (Appendix, Table 2). We use P and S wave arrival times to estimate locations for 10,617 earthquakes (Figure 3). Phase arrivals were identified using an initial run of automatic detection followed by manual pick adjustments. Our catalog for 2015-2016 is complete to a magnitude of 1.5, calculated using the ZMAP software package for MATLAB *[Wiemer, 2001]*, with many smaller earthquakes detected and included within the catalog.

Earthquakes were relocated using hypoDD *[Waldhauser, 2001]* (Appendix, Table 3). The RMS travel-time residuals of the events in the catalog decreased by approximately an order of magnitude, from ~0.17 sec to ~0.01 sec after relocation. To estimate the uncertainty in location, we ran hypoDD using velocities +/-5% the velocity model. We calculated the RMS location difference between the earthquake locations using each model, removing outliers more than 2 standard deviations from the mean difference. The horizontal RMS difference was 200 m and the depth difference was 130 m.

Using relocated earthquake locations, we identified regions of earthquake migration through time, and calculated migration rates by projecting earthquake

distance along a given fault and plotting distance vs. time. The average timing of earthquakes along the length of the fault was calculated in 200 m bins and weighted by the standard deviation of earthquake times within the bin. We then use a weighted least-squares inversion and boot-strap resampling to estimate the best-fitting migration velocity. The bootstrap method consisted of randomly resampling the data and performing the least-squares inversion, repeated in 5000 trials.

Focal mechanisms for 327 earthquakes of M1.78 to M4.24 were computed from P-wave first-motion polarities and S/P amplitude ratios using the HASH program *[Hardebeck & Shearer, 2002]*, using only earthquakes with >25 impulsive polarities (Figures 8,9; see Appendix Table 4). The HASH algorithm performs a grid search over all possible focal mechanisms to determine a set of acceptable focal mechanism solutions for each event. The nodal plane uncertainty is the RMS angular difference between the set of acceptable nodal planes and the preferred nodal plane; the average nodal plane uncertainty for our focal mechanism catalog is ~17°.

RESULTS

Overview of seismicity

Our seismic network in north-central Oklahoma provides an enhanced earthquake catalog (Figure 3) that includes 10,617 earthquakes ranging from local magnitude M-0.1 to M5.5. Our catalog contains nearly 10-fold more events than the USGS catalog for the same region within the same time frame of April 2015 through January 2016 *[ANSS]*. Earthquake depths are dominantly between 1.5 to 5 km depth (Figure 4), predominantly in granitic basement. During the time frame of our catalog, regions of seismic activity that began prior to our recording period expanded spatially at both the regional and individual-fault scale (Figure 7); earthquakes illuminated new faults in areas that had been inactive prior to our deployment, to the detection threshold of the USGS and OGS catalogs. The enhanced detection of low magnitude earthquakes in our catalog allows the identification of individual fault structures in the basement which had not previously been mapped.

Our catalog indicates a heterogeneous distribution of seismicity with earthquakes predominantly occurring on short unmapped structures of 2 km average length; few of the previously mapped faults coincide with well-defined seismic activity (Figure 3). The active faults that we identified from discrete seismic lineations range in orientation primarily from 45-95° with a subset ranging from 110-135° (Figure 5); the previously mapped fault segments which fall within that range have not been active during the period covered by our catalog, despite favorable orientation.

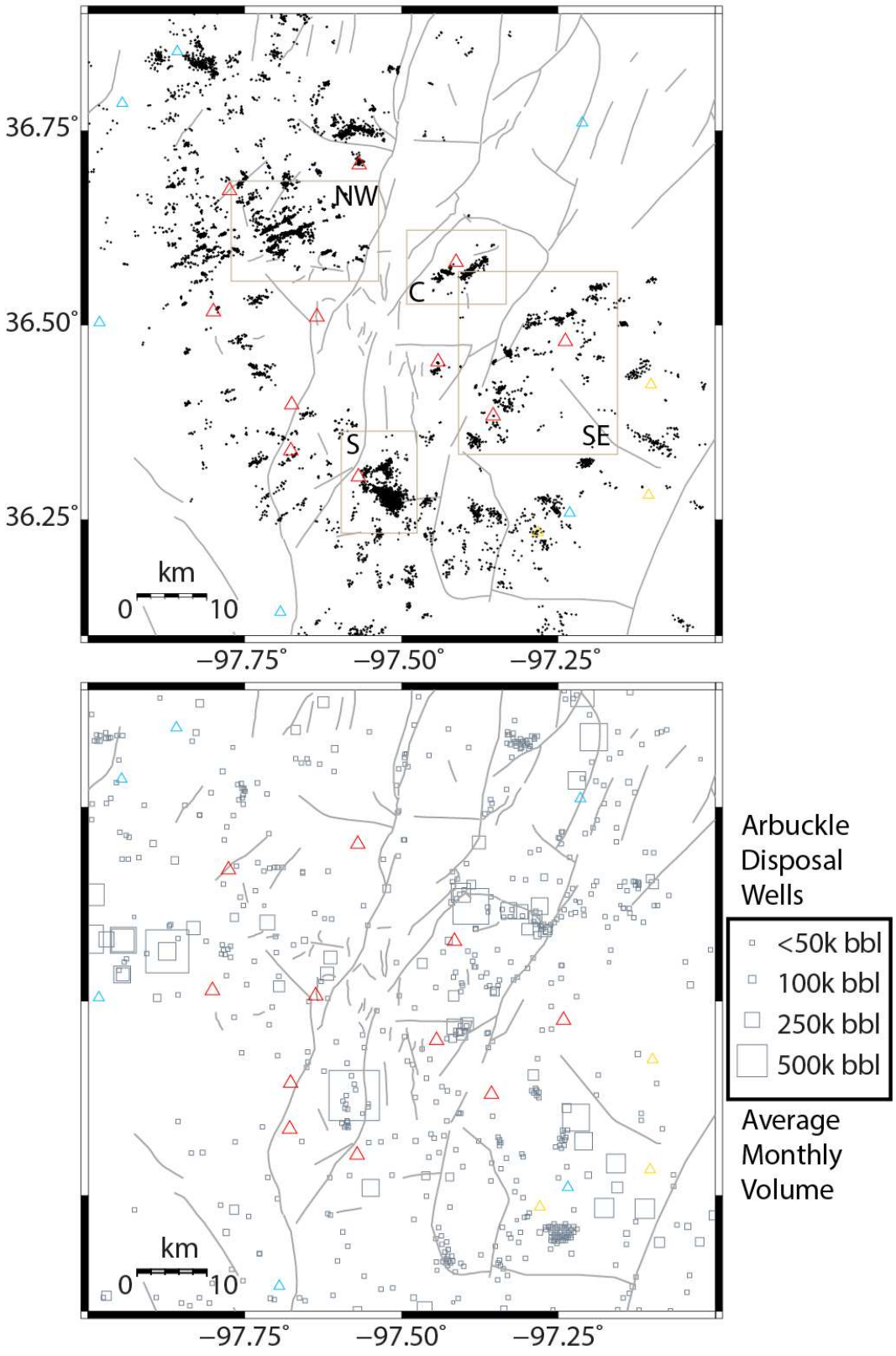
36.75°
36.50°
36.25°
NW
C
S
SE
km
0
10
−97.75°
−97.50°
−97.25°
Arbuckle
Disposal
Wells
<50k bbl
100k bbl
250k bbl
500k bbl
Average
Monthly
Volume

Figure 3. Seismicity and injection well locations in north-central Oklahoma. Station colors are as in Figure 1.

Above: Enhanced earthquake catalog; earthquake hypocenters are shown in black. Boxes indicate areas of interest discussed in the text in the northwest, southeast, central uplift, and south-central uplift.

Below: Locations of Arbuckle disposal wells indicated by squares, scaled by average monthly volume of injection.

Data source: Oklahoma Corporation Commission (OCC) UIC injection volumes, 2011-2015. Fault map from Marsh and Holland *[2016]*

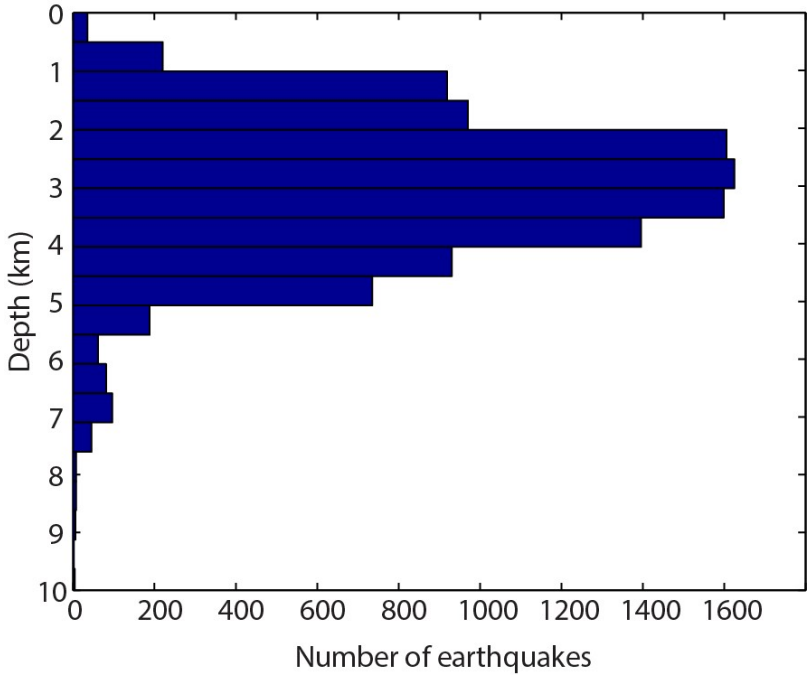

Figure 5. Earthquake depth histogram

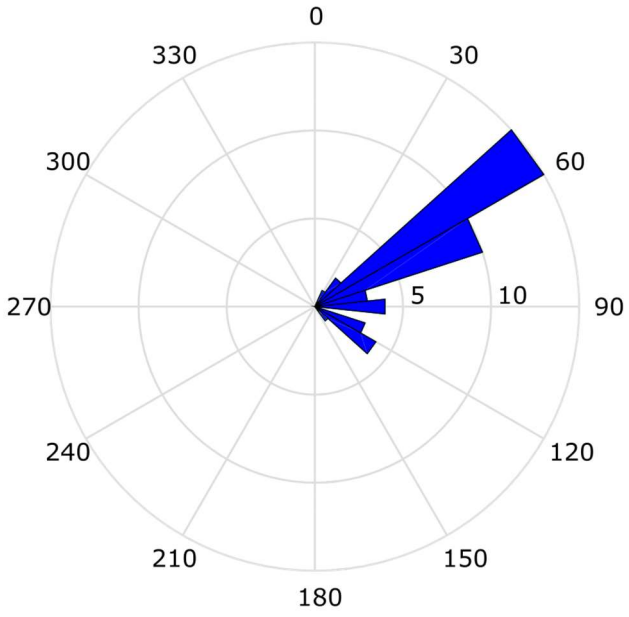

Figure 4. Orientation of previously unmapped faults traced from seismic lineations.

The majority of the earthquakes occur outside of the uplift on discrete faults throughout two broad areas, while activity within the uplift is concentrated in isolated clusters. We divide our results into four areas of interest (Figure 3) including two on the uplift flanks (northwest and southeast) and two within the uplift itself (central and south central).

Seismicity on uplift flanks

We first focus on the areas of interest outside of the uplift, to the northwest and southeast of the large border faults. Our catalog from April 2015 to January 2016 contains 1660 earthquakes of M-0.1-M4.2 on the northwest flank of the uplift, where earthquakes recorded by regional catalogs began in May 2013, prior to our array, and included 3 >M4.0 earthquakes. Seismicity in our catalog illuminates 10 subparallel faults at a predominant orientation of approximately 60°, with activated fault length ranging from 1.3 to 5 km (Figure 5). These faults are well-defined by the relocated earthquake locations, which demarcate 500-800 m wide fault zones. We note that the trend perpendicular to the dominant fault direction follows the dominant trend of joints and fractures in the region *[Liu et al., 1991]*. On some faults, earthquake activity occurred continuously throughout the period of our catalog; on others, seismicity moved throughout the region temporally via progressive failure along fault segments, or by jumping from fault to fault in sequence (Figure 7b). The short, subparallel faults, unmapped in publicly available data (e.g., Marsh and Holland, 2016), contain ~80% of activity in this area. Wells throughout this area range from monthly rates of 300 bbls to 250,000 bbls, with injection at five moderately sized wells (~100,000 to 250,000

bbl/month) beginning 2006-2015 *[OCC]*. The highest rate well (~250,000 bbl/month) began injection in June 2012 and is located <1 km from the western end of the largest active fault *[OCC]* (For full list of wells in NW area, see Appendix Table 5).

On the southeast flank of the uplift, earthquakes in our catalog define eight faults ranging between 1 to 2.8 km in length, at orientations ranging from 55° to 128°. The dominant strikes are between 55-65 degrees (37.5%) and 80-90 degrees (37.5%). Earthquakes on the southeast flank also occurred on unmapped faults. Seismic activity migrated temporally towards the uplift but our catalog does not indicate rupture on the previously mapped large faults delineating the border of the uplift. However, two clusters containing 129 earthquakes from M0.1 to M3.2 ruptured a subparallel fault, potentially a spur of the border fault, ~2 km east of the main fault (Figure 5). Monthly rates at injection wells in this area range from 350 bbls to 450,000 bbls per month; three moderate-to-large volume wells with rates of ~150,000 to ~450,000 bbls per month began injection in January 2012 and February and December 2013 *[OCC]* (Appendix Table 6).

In both areas on the flanks, seismicity defines networks of multiple faults in basement, often subparallel and spaced ~1-2 km apart. Earthquakes in these areas occurred near but did not cross the border faults, and seemingly did not occur on the main border faults. Earthquakes did not migrate continuously in one direction during the time period of the catalog in these areas, but instead ruptured individual faults, in cases rupturing progressively along the fault through time and or jumping between faults (Figure 7b,c).

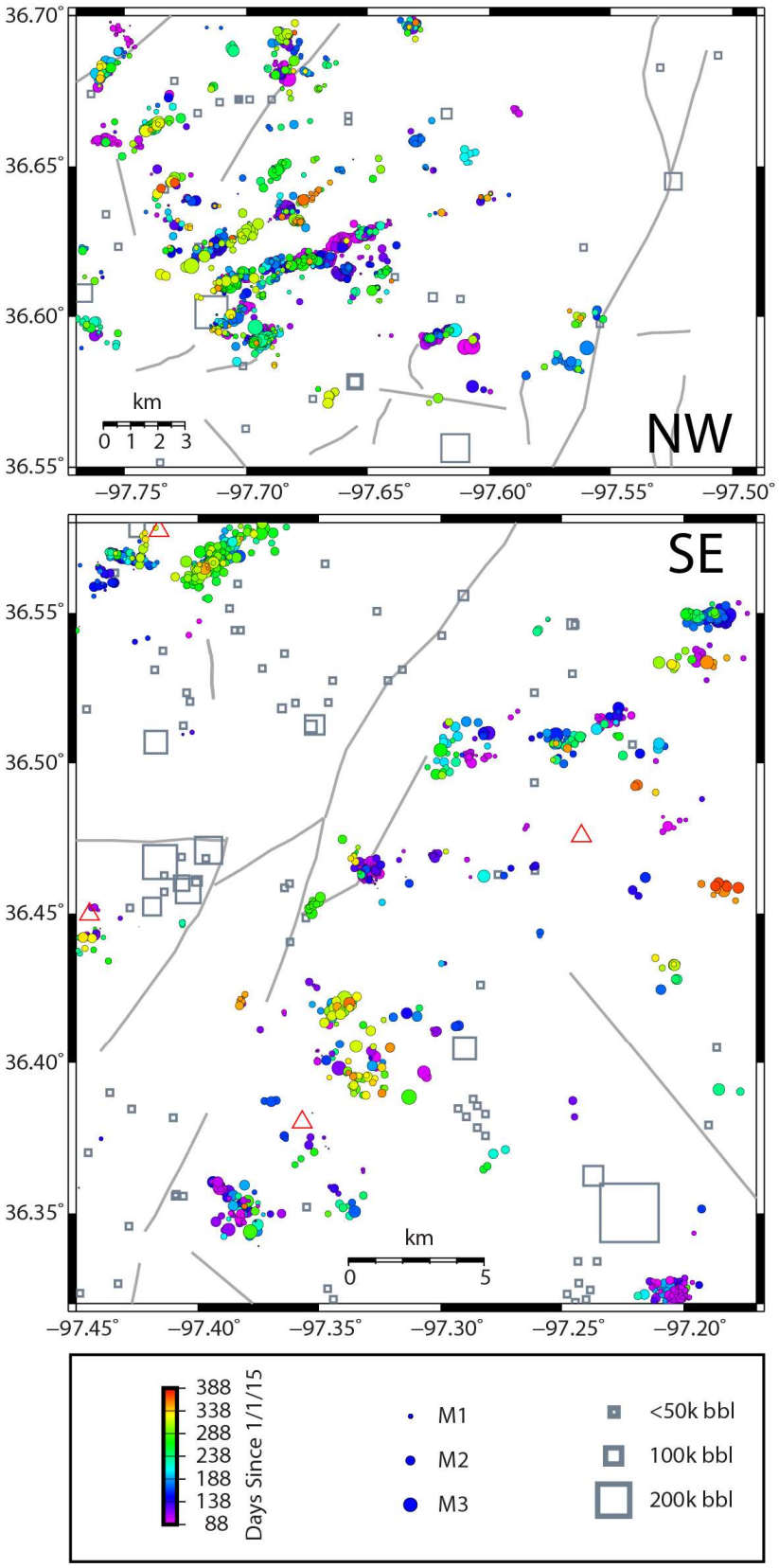
36.70°
36.65°
36.60°
36.55°
km
0 1 2 3
NW
−97.75°
−97.70°
−97.65°
−97.60°
−97.55°
−97.50°
SE
36.55°
36.50°
36.45°
36.40°
36.35°
km
0 5
−97.45°
−97.40°
−97.35°
−97.30°
−97.25°
−97.20°
388
338
288
238
188
138
88
Days Since 1/1/15
M1
M2
M3
<50k bbl
100k bbl
200k bbl

Figure 14. Seismicity on uplift flanks. Above: North-west area. Below: South-east area. Earthquake hypocenters are scaled by magnitude and colored by time. Wells in bold began injecting in 2015.

Data source: Oklahoma Corporation Commission (OCC) UIC injection volumes, 2011-2015. Fault map from Marsh and Holland *[2016]*.

Seismicity within the Nemaha uplift

In the center of the uplift, seismicity was not present in the USGS or OGS catalogs prior to the installation of our local seismometers in spring 2015. Earthquakes were recorded in this area beginning on March 30 in 2015, on a fault trending 110°, beginning initially on the northwest end and migrating east-southeast along the fault at a rate of ~25 m/day +/- 5 (Figure 7d). In mid-June 2015, earthquakes began on a nearby, 50° trending, unmapped fault 1.5 km east of the initial fault, and migrated to the northeast and southwest along the fault, again at a rate of ~25 m/day (Figure 7e). A moderate size (~120,000 bbl/month) injection well is located 1.4 km to the northeast of the initial fault; injection began at this well in October of 2012. Additional wells (70,000 to 90,000 bbl/month) that began injection in January and July of 2012 are located immediately to the north of the second fault; a fourth well located 3.5 km to the southwest of the first fault is the highest rate well within 4 km at ~160,000 bbl per month *[OCC]* (Appendix Table 7). There is little to no other seismicity surrounding this area for >10km (Figure 3).

At the southern end of the uplift, two seismic clusters occurred, including 4 M>4.0 earthquakes and >100 M3.0 earthquakes since 2014 *[ANSS]*. Two of these >M4.0 earthquakes occurred during the time period covered by our catalog. This region is structurally complex, as it is immediately north of the transition from the uplift bounded by multiple large faults to a single Nemaha fault. Earthquakes in this area occur primarily on two previously unmapped faults at 59° and 118° orientations

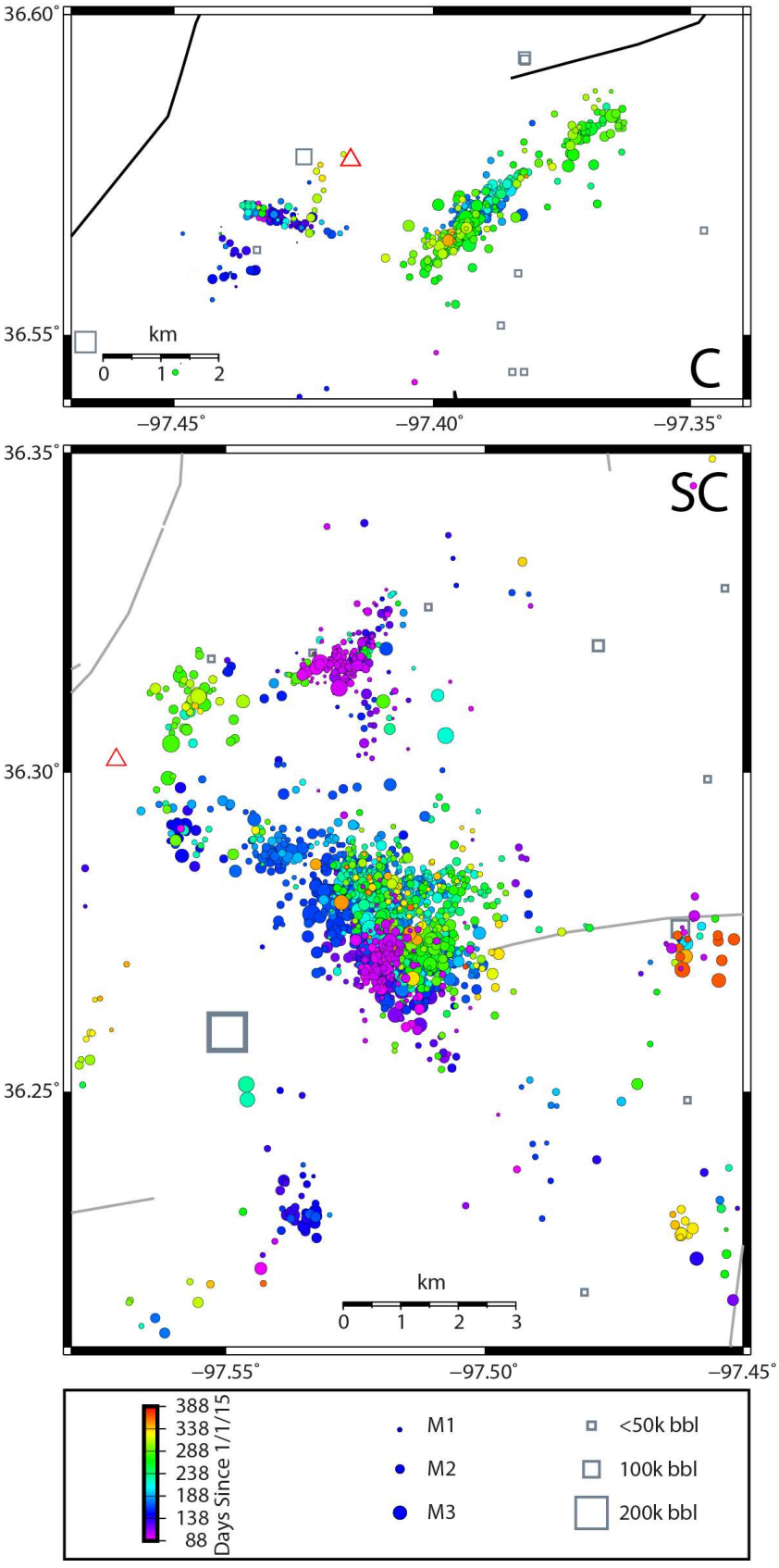
36.60°
36.55°
km
0 1 2
C
−97.45°
−97.40°
−97.35°
36.35°
SC
36.30°
36.25°
km
0 1 2 3
−97.55°
−97.50°
−97.45°
388
338
288
238
188
138
88
Days Since 1/1/15
M1
M2
M3
<50k bbl
100k bbl
200k bbl

Figure 15. Seismicity within the uplift. Earthquake hypocenters are scaled by magnitude and colored by time. Wells in bold began injecting in 2015. Above: Central uplift. Below: South-central uplift.

Data source: Oklahoma Corporation Commission (OCC) UIC injection volumes, 2011-2015. Fault map from Marsh and Holland *[2016]*.

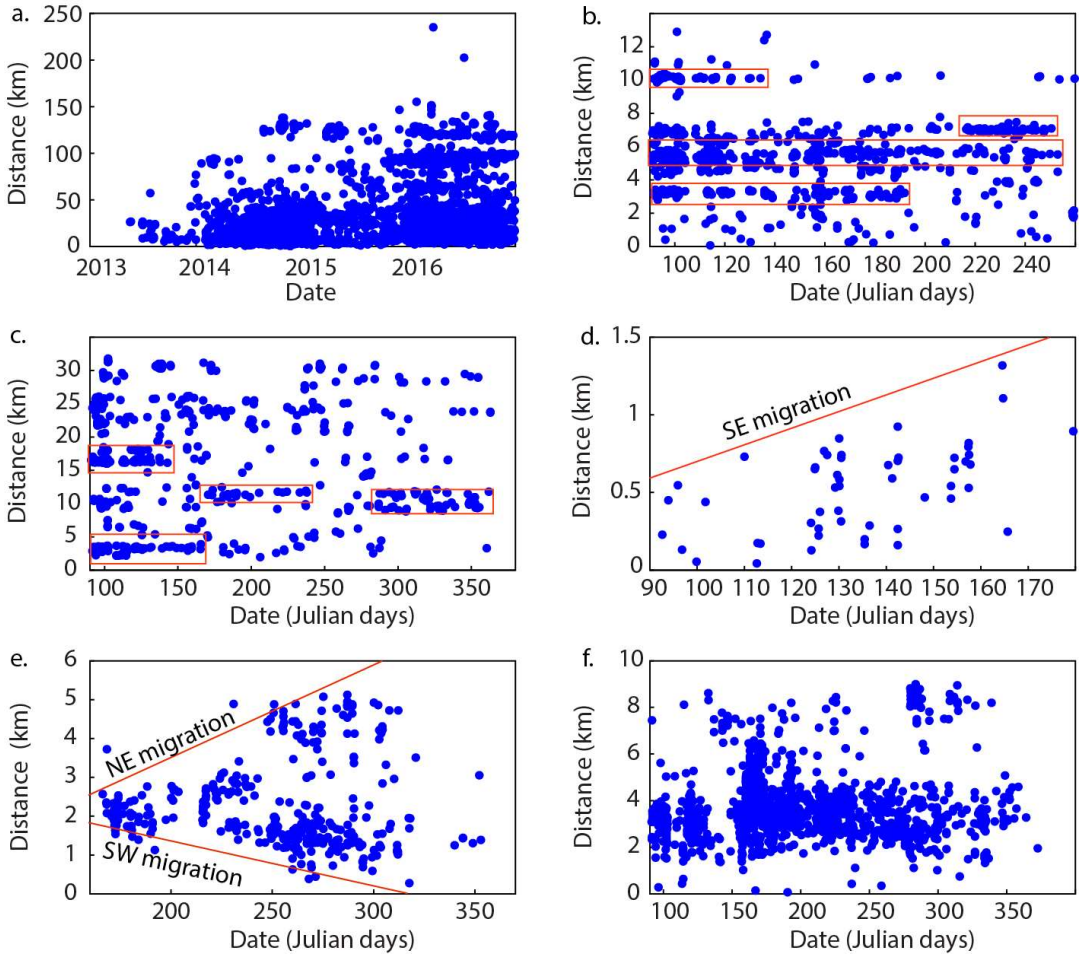

Figure 16. Migration patterns over time. **a.** Earthquakes in the north-central area of seismic activity recorded by the USGS, 2013-2016. Distance is calculated from the center point of the area of active seismicity, showing expansion of the area over time. **b,c.** Earthquakes over time in the NW and SW areas. Distance is projected along a line perpendicular to the fault network. Individual faults (indicated in red boxes) may be active throughout the time period recorded, or become active progressively. **d,e.** Migration over time on fault 1 (**d**) and fault 2 (**e**) in the central uplift. Distance is projected along the fault, showing migration to the SE on fault 1 and simultaneous migration to the NE and SW on fault 2. **f.** Earthquakes over time in the south-central uplift. Distance is projected along-fault. No trend in migration over time is evident.

Data source: ANSS Earthquake Catalog, USGS (subplot a).

(Figure 6). Unlike the other primarily vertical faults in our area, the northern, 59° trending fault dips steeply to the SE, with depths ranging from 2-8 km. On the southern fault, earthquake depths range from 2-5 km over a width of 2.5-3 km. Three moderate sized injection wells (~80,000-290,000 bbl per month) are located within 3.5 km of either fault, with injection beginning at these wells in August 2013 and October 2014 east of the faults, and in July 2014 for the well to the southwest, the highest-rate well within 8 km *[OCC]* (Appendix Table 8).

Within both of these areas in the uplift, most of the seismicity occurred within discrete zones, delineating previously unmapped faults, as did the seismicity in the zones on either side of the uplift. The primary difference between seismicity within the uplift compared to the surrounding regions is the distribution; within the uplift, the seismicity occurs on isolated, conjugate fault pairs near wells.

Focal mechanisms

The focal mechanism solutions across our study area are predominantly high angle strike-slip mechanisms (96%), with 4% percent normal events. Outside the uplift, the focal mechanisms in the northwest are majority right-lateral strike-slip (Figure 8); ~6% in this area are normal mechanisms. Nodal planes are predominantly oriented at ~60° and ~150°. The majority of normal mechanisms are oriented at 150° on one fault at a perpendicular trend to the strike-slip mechanisms. Mechanisms to the southeast (Figure 8) are also dominantly strike-slip; only ~4% are normal faulting earthquakes. Nodal plane orientations range from 0° to 155° and lack a dominant orientation.

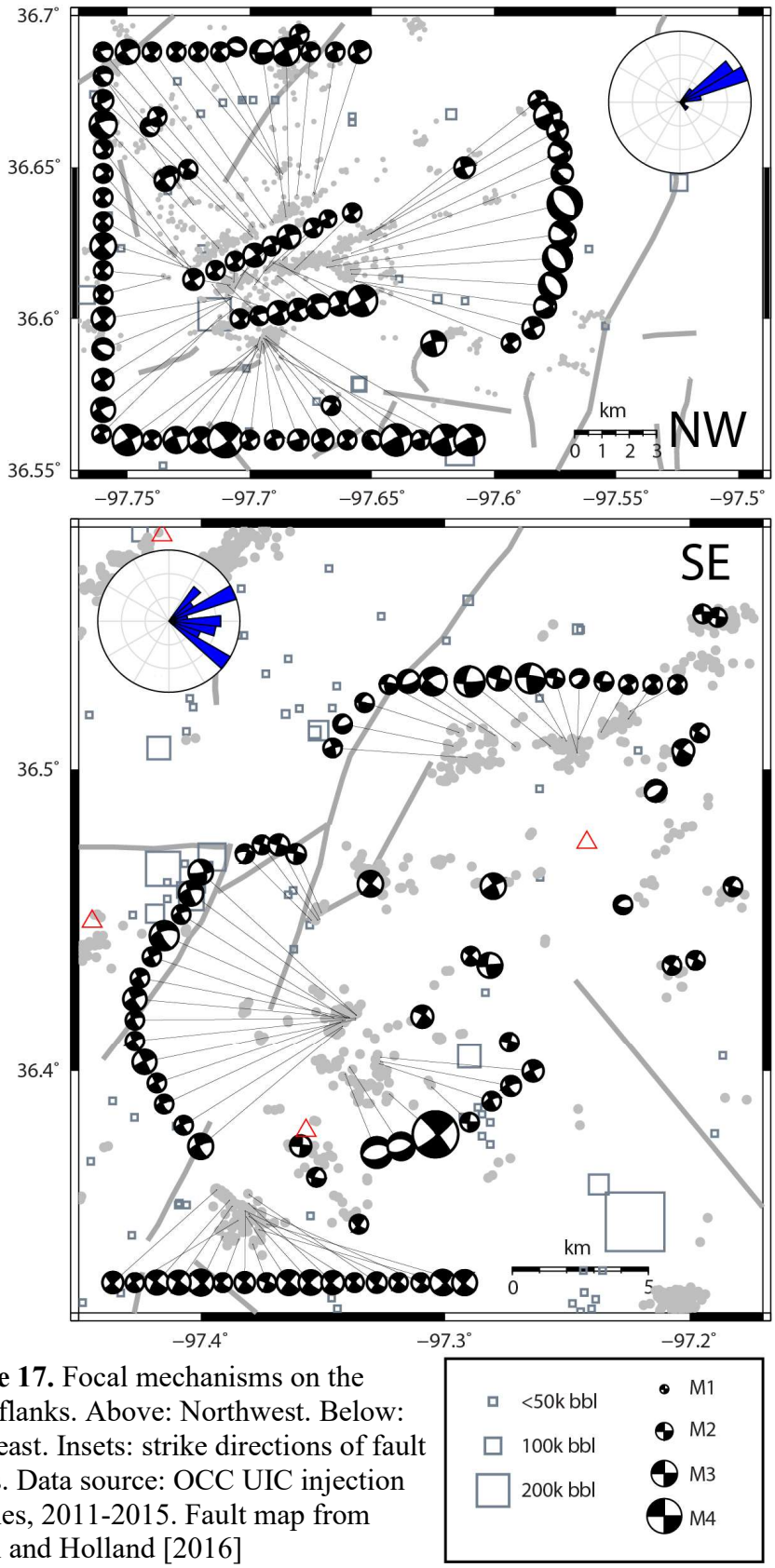

Figure 17. Focal mechanisms on the uplift flanks. Above: Northwest. Below: Southeast. Insets: strike directions of fault planes. Data source: OCC UIC injection volumes, 2011-2015. Fault map from Marsh and Holland [2016]

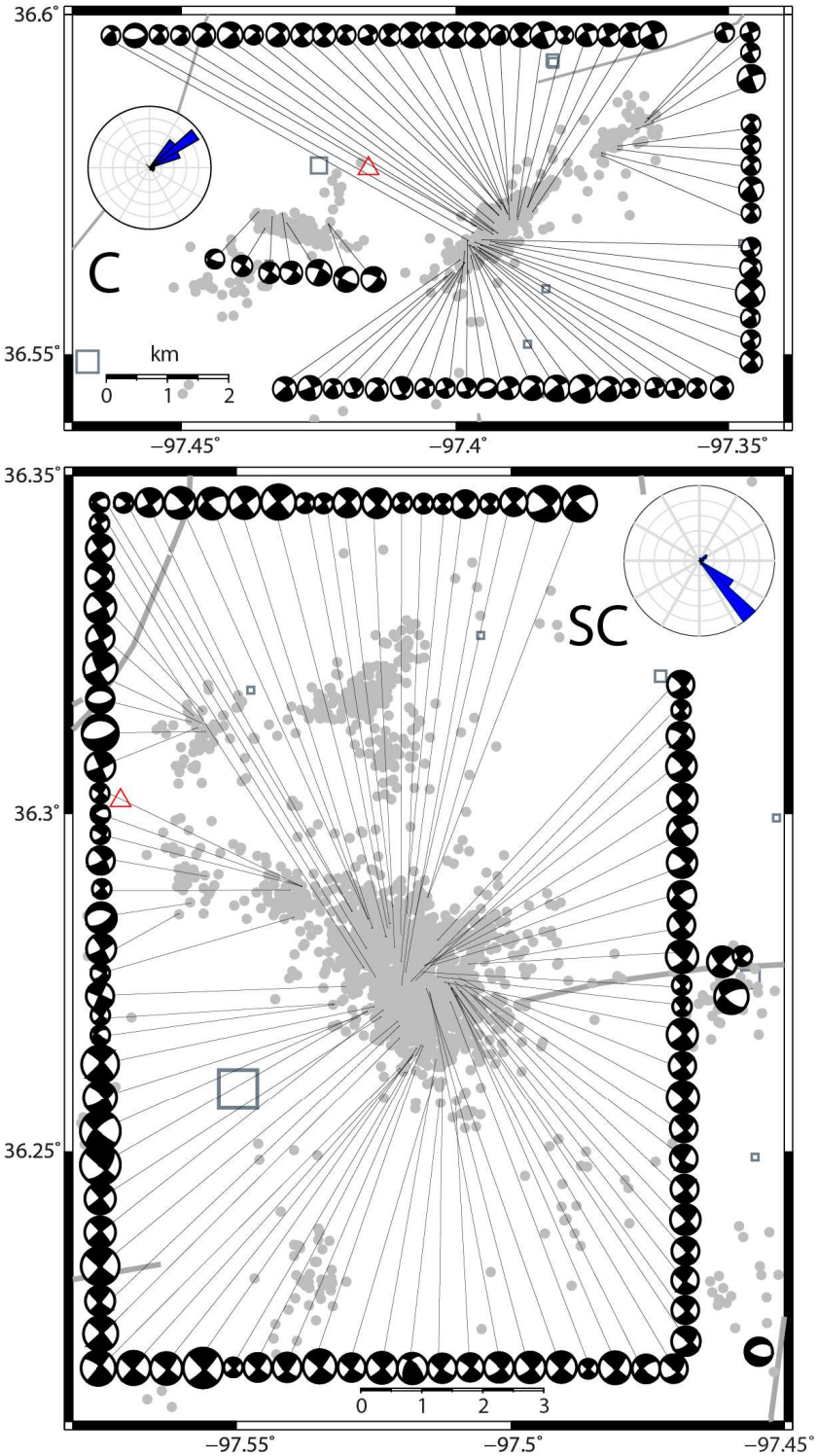

Figure 18. Focal mechanisms within the uplift. Above: Central uplift. Below: South-central uplift. Insets: strike directions of fault planes. Data source: OCC UIC injection volumes, 2011-2015. Fault map from Marsh and Holland *[2016]*

Within the central uplift, focal mechanisms are predominantly strike-slip (Figure 9), with left lateral motion on the western, 110° trending fault, and right lateral motion on the eastern, 50° trending fault. Approximately 3% of mechanisms are normal faulting. Nodal planes strikes are predominantly ~55° and ~145°. In the southern uplift, strike-slip focal mechanisms are right lateral on the northern fault and left lateral on the southern; ~4% of mechanisms are normal faulting. The nodal plane strikes are narrowly clustered around 45° and 135° (Figure 9).

DISCUSSION

Using our newly developed earthquake catalog with enhanced detection of low magnitude events, we are able to identify active fault structures in and around the Nemaha uplift, an area of considerable interest for hazard assessment due to the presence of long (>100km) fault segments in Oklahoma. Here we show that these earthquakes largely occur on dense networks of small, unmapped, pervasive faults, and do not occur on faults mapped in the sedimentary section. Within the uplift, seismic activity is constrained to discrete faults near injection wells. Seismicity does not occur near the high injection rate areas within the uplift; rather, the seismicity occurs near smaller wells which are in the center of the uplift, further from the large mapped faults.

The identification of previously unmapped faults through our enhanced local catalog allows us to understand structures within the basement at a scale that no individual study in this area has allowed before. Previous studies of the geology of north-central Oklahoma *[e.g., Cary, 1955; Chandler, 1979; Clark & Cooper, 1927; Clark & Daniels, 1927; Dana, 1955; Page, 1955; Shelton et al., 1979; Wallace, 1964]* are generally localized to scales ranging from a single township to a county and are focused on the sedimentary section. Marsh and Holland *[2016]* synthesized the faults available in published literature into a map of known faults in Oklahoma, but as our work shows, these mapped faults are not sufficient to delineate basement structures hosting seismicity. Using seismicity to image unmapped basement structures shows

the benefit of our detailed low-magnitude catalog in determining the distribution of fault and fracture systems in the basement.

The identification of active basement structures also reveals the variation in seismicity across the uplift described above. We propose a model of variable fault density, fracturing, and resulting permeability structure across the uplift to explain the seismic variability. The large faults bounding the uplifted structures may serve as permeability baffles to the regional pressure pulse, isolating the uplift by impeding fluid migration into the uplift. Within the uplift, dense secondary faulting and fracturing within the zone of transpression may allow rapid fluid dissipation, inhibiting fluid pressures due to local injection from reaching critical levels.

Fault zone structure and permeability

Fault zones have the potential to strongly modulate fluid flow in the shallow crust *[Faulkner et al., 2010; Wibberley et al., 2008]*. In a typical fault, strain is localized with a fault core surrounded by a peripheral damage zone of fractures and subsidiary faults up to hundreds of meters wide *[Faulkner et al., 2010; Savage & Brodsky, 2011; Vermilye & Scholz, 1998]*. Though the impact on permeability is variable depending upon the fault structure *[Caine, Evans, & Forster, 1996]*, the fault core can impede across-fault flow, whereas fault damage zones can be along-fault flow conduits. The geometry of fault offsets can also create barriers or conduits for across-fault flow, depending upon the contrast of rock types; reservoir-to-sealing-lithology connections will create a side-seal at the fault, while reservoir to reservoir connections may create a cross-fault pathway *[Wibberley et al., 2008]*. Discontinuities

created by the high-length, large-offset border faults of the Nemaha Uplift may be acting as barriers or baffles to fluid flow into the center of the uplift if the fault offset juxtaposes reservoir rocks against sealing lithologies, or if low permeability fault gouge interrupts reservoir-reservoir connections.

The internal structure of the Nemaha uplift, a wrench zone of multiple faults over 650 km, is pervasively faulted and fractured, and potentially chemically altered *[McBee, 2003; Scott & McElroy, 1964; Stevens et al., 2016; Walters, 1953]*. North of our study area, Precambrian crystalline basement in Kansas is altered *[Scott & McElroy, 1964]*, and structural highs in basement are fractured *[Walters, 1953]*. Fractured basement highs produce oil in central Kansas, with fractures serving as the reservoirs *[Walters, 1953]*. Tomographic imaging within the Nemaha uplift in Oklahoma indicates a low velocity anomaly within the uplift, consistent with heavily fractured or altered basement within the Nemaha uplift *[Stevens et al, 2016]*.

Conceptual model of fault zone permeability and fluid pressures

We interpret the low level of seismicity within the uplift as the result of fault zone controls on permeability (Figure 12). The large faults of the uplift serve as low-permeability baffles which buffer the uplift from the effects of regional pressurization. The fractured and faulted basement within the uplift likely enhances permeability and provides more efficient fluid pathways to dissipate fluid pressure. The effect of local fluid injection within the uplift may thus be modulated by this efficient pressure dissipation; therefore, even though the basement has fractures abundantly available,

fluid pressures do not reach critical levels, and seismicity is rare, except on faults near wells, before fluid pressure dissipates.

Externally, regional fluid pressurization triggers earthquakes throughout a network of fractures in basement. Despite the less pervasive nature of these fractures as compared to the faults we interpret to be present within the uplift, the fractures are nonetheless spaced at ~2 km apart. The average length of an activated fault is short, likely indicating non-continuous segments of basement faults hosting the earthquakes. Poorly oriented fracture sets may serve as aseismic fluid pathways between well-oriented faults. In comparison, the fault and fracture systems within the uplift, associated with the long faults of the Nemaha uplift and their more extensive damage zones, are more likely to form interconnected, continuous systems of fractures which act as more efficient fluid pathways. The pervasive, short-length faults in basement outside of the uplift represent a case that lies between endmember situations of low fracturing/low permeability and high fracturing/high permeability. In the case of limited fracturing and low permeability, fluid would not be able to migrate through the subsurface, and seismicity would be limited. In areas of enhanced fracturing, fluid would migrate too rapidly for high fluid pressures to build up, as we interpret within the uplift. Pervasive but non-continuous basement fractures represent a midpoint between these cases, where less efficient fluid pathways focus fluids along narrow fractures, increasing local fluid pressures and resulting in elevated seismicity levels.

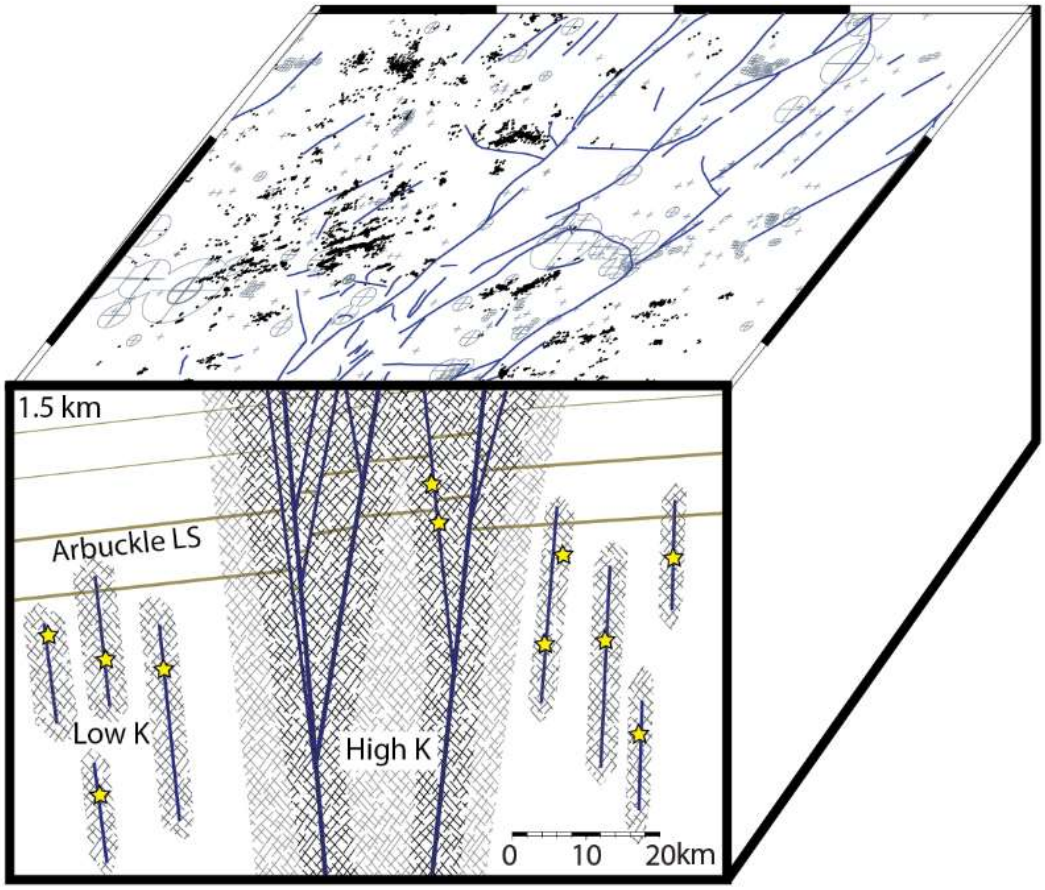

Figure 11. Conceptual model of fault and fracture density. Cross-section demonstrates variation in fault and fracture density and permeability structure across the uplift, showing low permeability and increased seismicity (stars) in the uplift flanks compared to the uplift. Upper surface represents a projection of earthquake hypocenters, mapped faults, and surface well locations onto ~1.5 km depth.

Data source: OCC UIC injection volumes, 2011-2015. Fault map from Marsh and Holland *[2016]*.

CONCLUSIONS

The spatio-temporal evolution of earthquakes in the north Oklahoma seismic gap emphasizes the influence of structural setting in mediating regional fluid pressurization. The Nemaha fault zone and its position between expanding centers of seismicity provided the opportunity to investigate the seismic response across the fault zone structure, as characterized by our local earthquake catalog. We found that the majority of earthquakes occur away from the major structures of the Nemaha uplift, on widely distributed, small offset faults. Within the uplift, events occur in discrete clusters on isolated faults near wells. Variations in fault density, fracturing, and permeability structure across the fault zone structure provide structural controls on fluid pressure migration and on seismicity patterns. We propose that the numerous small-offset faults on the flanks of the uplift are less efficient fluid pathways, perhaps less continuous, resulting in higher fluid pressure and a higher seismicity rate. The highly fractured basement of the uplift may dissipate fluid pressure more readily and thus inhibit widespread seismicity.

The prevalence of seismicity on unmapped faults presents a challenge for methods of hazard analysis which depend on maps of known faults. Faults of the Nemaha uplift mapped in the sedimentary section are not adequate for characterizing basement structures not expressed in sediment. Outside of the Nemaha, previously unknown faults also hosted the Pawnee M5.8 event in September 2016 and the M5.7 mainshock in Prague in November 2011, which occurred on a then-unmapped spur of the Wilzetta Fault. These events were the largest recorded earthquakes in the state of

Table 1. Fault planes and stress orientations at prominent sites of induced seismicity.

Site	Stress orientation	Fault plane	Angle between fault plane and stress	Injection pressure
Rangely, CO	70° *[Raleigh et al., 1972]*	50° *[Raleigh et al., 1972]*	20°	27.5 MPa *[Raleigh et al., 1972]*
Snyder, TX	64° *[Heidbach et al., 2010]*	80° *[Voss & Herrmann, 1978; Herrmann 2016]*	16°	38 MPa *[Davis & Pennington, 1989]*
Paradox Valley, CO	110° *[Ake et al, 2005]*	86° 125° *[Ake et al., 2005]*	24° 15°	~82 MPa *[Ake et al.,2005]*
Rocky Mountain Arsenal, CO	~165° *[Heidbach et al., 2010]*	130° *[Herrmann et al., 1981]*	35°	36 MPa *[Healy et al., 1968]*

Oklahoma, showing that the presence of unmapped structures has significant implications for hazard. Our enhanced local catalog, which allows imaging of unmapped basement faults and fracture sets across our study area, provides a better understanding of basement structure and of the geologic complexities controlling injection-induced seismicity.

Though the large border faults of the Nemaha uplift have not experienced seismic activity, several active faults cross-cut the western border fault, and our results show that the regions around the border faults host earthquakes and thus are likely impacted by perturbed fluid pressure. We also see poorly oriented faults failing in the regions outside the uplift, suggesting that failure on the large, poorly oriented border faults remains a possibility. In other well-documented examples of induced seismicity, the Rangely and Paradox Valley sequences in Colorado and the Cogdell oil field sequence in Texas included rupture on poorly to moderately oriented faults (Table 1) *[Ake et al., 2005; Davis & Pennington, 1989; Raleigh et al., 1972]*. Within Oklahoma, the Prague sequence in 2011 also included failure on a poorly oriented fault, as progressive rupture of three fault planes began on well-oriented faults but propagated onto a third, poorly oriented plane *[Keranen et al., 2013]*. In other cases such as Rocky Mountain Arsenal, Colorado *[Healy et al., 1968; Herrmann et al., 1981]*, as well as in the 2016 Pawnee earthquake in Oklahoma, induced earthquakes occur on well-oriented faults. Though seismicity within the Nemaha uplift appears to be modulated via our proposed fractured uplift model, the border faults of the uplift are subject to ongoing pressurization and may still present a potential hazard to north-central Oklahoma despite being poorly oriented.

WORKS CITED

Ake, J., Mahrer, K., O'Connell, D., & Block, L. (2005). Deep-injection and closely monitored induced seismicity at Paradox Valley, Colorado. *Bulletin of the Seismological Society of America*, *95*(2), 664–683. https://doi.org/10.1785/0120040072

Caine, J. S., Evans, J. P., & Forster, C. B. (1996). Fault zone architecture and permeability structure. *Geology*, *24*(11), 1025. https://doi.org/10.1130/0091-7613(1996)024<1025:FZAAPS>2.3.CO;2

Cary, L. W. (1955). The subsurface geology of the Garber area, Garfield county, Oklahoma. *The Shale Shaker Digest*, *5*, 384–403.

Chandler, C. E. (1979). Subsurface Stratigrapic Analysis of Selected Sandstones of the, 1–16. Retrieved from http://archives.datapages.com/data/ocgs/data/009/009001/0001.htm

Clark, G. C., & Cooper, O. L. (1927). Oil and Gas in Oklahoma: Oil and Gas Geology of Kay, Grant, Garfield, and Noble Counties. *Bulletin of the Oklahoma Geological Survey*, *40–H*. Retrieved from http://ogs.ou.edu/docs/bulletins/B40-H.pdf

Clark, S. K., & Daniels, J. I. (1927). RELATION BETWEEN STRUCTURE AND PRODUCTION IN THE MERVINE , PONCA , BLACKWELL , AND SOUTH BLACK- KAY COUNTY , OKLAHOMA The geologic sections encountered in each of the fields and their cor- relations are shown by the type logs in Figure 2 . The history of.

Dana, G. F. (1955). The subsurface geology of Grant county, Oklahoma, 32–48.

Davis, S. D., & Pennington, W. D. (1989). Induced seismic deformation in the Cogdell oil field of west Texas. *Bulletin of the Seismological Society of America*, *79*(5), 1477–1495. Retrieved from http://www.bssaonline.org/content/79/5/1477.short

Dolton, G. L., & Finn, T. M. (1989). Petroleum geology of the Nemaha Uplift, central mid-continent. *U.S. Geological Survey Open-File Report 88-450D*, 39.

Ellsworth, W. L. (2013). Injection-induced earthquakes. *Science*, *341*(6142), 1225942. https://doi.org/10.1126/science.1225942

Faulkner, D. R., Jackson, C. A. L., Lunn, R. J., Schlische, R. W., Shipton, Z. K., Wibberley, C. A. J., & Withjack, M. O. (2010). A review of recent developments concerning the structure , mechanics and fl uid fl ow properties of fault zones. *Journal of Structural Geology*, *32*(11), 1557–1575. https://doi.org/10.1016/j.jsg.2010.06.009

Gay, S. Parker, J. (2003a). The Nemaha Trend-A System of Compressional Thrust-Fold, Strike-Slilp Structural Features in Kansas and Oklahoma, Part 1. *Shale Shaker*.

Gay, S. Parker, J. (2003b). The Nemaha Trend-A System of Compressional Thrust-Fold, Strike-Slilp Structural Features in Kansas and Oklahoma, Part 2. *Shale Shaker*, (October), 9–49.

Hardebeck, J. L., & Shearer, P. M. (2002). A New Method for Determining First-Motion Focal Mechanisms. *Bulletin of the Seismological Society of America*, *92*(6), 2264–2276. https://doi.org/10.1785/0120010200

Healy, J. H., Rubey, W. W., Griggs, D. T., & Raleigh, C. B. (1968). The Denver Earthquakes. *Science*, *161*. Retrieved from http://cogcc.state.co.us/documents/library/Technical/Induced Seismicity/Healy_et_al_1968_Science.pdf

Heidbach, O., Tingay, M., Barth, A., Reinecker, J., Kurfeß, D., & Müller, B. (2010). Global crustal stress pattern based on the World Stress Map database release 2008. *Tectonophysics*, *482*(1–4), 3–15. https://doi.org/10.1016/j.tecto.2009.07.023

Herrmann, R. B., Park, S.-K., & Wang, C.-Y. (1981). The denver earthquakes of 1967-1968. *Bulletin of the Seismological Society of America*, *71*(3), 731–745. Retrieved from http://www.bssaonline.org/content/71/3/731.abstract

Keranen, K. M., Savage, H. M., Abers, G. A., & Cochran, E. S. (2013). Potentially induced earthquakes in Oklahoma, USA: Links between wastewater injection and the 2011 Mw 5.7 earthquake sequence. *Geology*, *41*(6), 699–702. https://doi.org/10.1130/G34045.1

Keranen, K., Weingarten, M., & Abers, G. (2014). Sharp increase in central Oklahoma seismicity since 2008 induced by massive wastewater injection. *Science*, *345*(6195), 448–451. https://doi.org/10.1038/45144

Liu, E., Crampin, S., & Queen, J. H. (1991). Fracture detection using crosshole surveys and reverse vertical seismic profiles at the Conoco Borehole Test Facility, Oklahoma. *Geophysical Journal International*, *107*(3), 449–463. https://doi.org/10.1111/j.1365-246X.1991.tb01406.x

Marsh, S., & Holland, A. (2016). Comprehensive Fault Database and Interpretive Fault Map of Oklahoma. *Klahoma Geological Survey Open File Report OF2-2016*.

McBee, W. (2003). Nemaha Strike-Slip Fault Zone, *10055*.

Morgan, B. C., & Murray, K. E. (2015). Characterizing Small-Scale Permeability of

the Arbuckle Group, Oklahoma. *Oklahoma Geological Survey Open File Report*, *OF2-2015*(January), 1–12. https://doi.org/10.13140/2.1.3512.6569

Page, K. G. (1955). The Subsurface Geology of Southern Noble County, Oklahoma, 448–466. Retrieved from http://archives.datapages.com/data/ocgs/data/001/001001/0448.htm

Raleigh, C. B., Healy, J. H., & Bredehoeft, J. D. (1972). Faulting and Crustal Stress at Rangely, Colorado. *Flow and Fracture of Rocks*, *16*, 275–284. https://doi.org/10.1029/GM016p0275

Savage, H. M., & Brodsky, E. E. (2011). Collateral damage: Evolution with displacement of fracture distribution and secondary fault strands in fault damage zones. *Journal of Geophysical Research: Solid Earth*, *116*(3). https://doi.org/10.1029/2010JB007665

Scott, R. W., & McElroy, M. N. (1964). Precambrian-Paleozoic Contact in Two Wells in Northwestern Kansas. *Kansas Geological Survey Bulletin*, *170*(2). Retrieved from http://www.kgs.ku.edu/Publications/Bulletins/170_2/

Shah, A. K., & Keller, G. R. (2017). Geologic influence on induced seismicity: Constraints from potential field data in Oklahoma. *Geophysical Research Letters*, *44*(1), 152–161. https://doi.org/10.1002/2016GL071808

Shelton, J. W., Jenkins, W. A., & Bingham, R. H. (1979). Geology and mineral resources of Noble County, Oklahoma. Bulletin of the Oklahoma Geological Survey.

Stevens, N. T., Keranen, K. M., & Lambert, C. (2016). Double-difference tomography velocity structure in Northern Oklahoma: Evidence for reduced. In *American Geophysical Union*. https://doi.org/10.1785/0120020190

Vermilye, J. M., & Scholz, C. H. (1998). The process zone: A microstructural view of fault growth. *Journal of Geophysical Research-Solid Earth*. https://doi.org/10.1029/98JB00957

Voss, J. A., & Herrmann, R. B. (1978). A surface wave study of the June 16, 1978 Texas earthquake. *Earthquake Notes*, *51*(1). Retrieved from http://srl.geoscienceworld.org/content/gssrl/51/1/1.full.pdf

Waldhauser, F. (2001). HypoDD - A Program to Compute Double-Difference Hypocenter Locations by. *US Geol. Surv. Open File Rep. 01-113*, 1–25. https://doi.org/http://geopubs.wr.usgs.gov/open-file/of01-113/

Wallace, N. (1964). The Billings Field, Noble County, Oklahoma, *32*, 152–155. Retrieved from http://archives.datapages.com/data/tgs/digest/data/032/032001/152_tgs320152.ht

m

Walters, R. F. (1953). Oil Production from Fractured Pre-Cambrian Basement Rocks in Central Kansas. *AAPG Bulletin*, *37*. https://doi.org/10.1306/5CEADC59-16BB-11D7-8645000102C1865D

Weingarten, M., Ge, S., Godt, J. W., Bekins, B. a, & Rubinstein, J. L. (2015). High-rate injection is associated with the increase in U.S. mid-continent seismicity. *Science*, *348*(6241), 1336–1340. https://doi.org/10.1126/science.aab1345

Wibberley, C. A. J., Yielding, G., Toro, G. Di, Wibberley, C. A. J., Yielding, G., Toro, G. D. I., … Pe, L. (2008). Recent advances in the understanding of fault zone internal structure : a review. *Geological Society , London, Special Publication*, 5–33. https://doi.org/10.1144/SP299.2

Wiemer, S. (2001). A Software Package to Analyze Seismicity: ZMAP. *Seismological Research Letters*, *72*(3). Retrieved from http://srl.geoscienceworld.org/content/72/3/373

Yeck, W. L., Weingarten, M., Benz, H. M., Mcnamara, D. E., Bergman, E., Herrmann, R. B., … Earle, P. S. (2016). Far-field pressurization likely caused one of the largest injection induced earthquakes by reactivating a large pre-existing basement fault structure. *Geophysical Research Letters*. https://doi.org/10.1002/2016GL070861

APPENDIX

Table 2. List of stations used in earthquake catalog

Name	Net	Lat	Long	Elev (m)	Sensor	Sample Rate (sps)	Deployed
EA01	CU	36.5140	-97.8021	354	Trillium Compact	250	3/31/2015
EA02	CU	36.4497	-97.4445	311	Trillium Compact	250	3/31/2015
EA03	CU	36.7022	-97.5702	310	Trillium Compact	250	3/31/2015
EA04	CU	36.3020	-97.5713	352	Trillium Compact	250	3/29/2015
EA05	CU	36.6692	-97.7765	318	Trillium Compact	250	4/1/2015
EA06	CU	36.5073	-97.6373	320	Trillium Compact	250	3/31/2015
EA07	CU	36.3946	-97.6775	348	Trillium Compact	250	3/31/2015
EA08	CU	36.5773	-97.4159	318	Trillium Compact	250	3/30/2015
EA09	CU	36.4758	-97.2420	282	Trillium Compact	250	3/30/2015
EA10	CU	36.3803	-97.3570	332	Trillium Compact	250	3/29/2015
EA11	CU	36.3354	-97.6789	360	Trillium Compact	250	7/29/2015
BCOK	OK	35.6567	-97.6093	302	CMG3-ESP	100	2/9/2013
BLOK	OK	36.7606	-97.2150	301	CMG6T	100	5/27/2015
CROK	OK	36.5047	-97.9834	403	CMG3-ESP	100	8/7/2013
GC02	OK	36.8515	-97.8596	354	HS-1	100	11/5/2014
GORE	OK	36.7856	-97.9471	348	Trillium Compact	200	5/27/2015
KAY1	OK	36.7627	-97.2122	309	Trillium Compact	200	3/26/2014
QUOK	OK	36.1714	-96.7080	296	CMG6T	100	3/28/2014
U32A	OK	36.3795	-99.0014	525	STS2	100	2/24/2012
KNG1	ZD	36.1323	-97.6955	298	L22	200	4/1/2014
A005	OKSTU	36.2350	-97.2798	300	CMG6T	100	9/14/2014
A008	OKSTU	36.2829	-97.1038	304	CMG6T	100	10/24/2014

A011	OKSTU	36.4252	-97.1000	291	CMG6T	100	3/29/2015
KAN13	GS	37.0129	-97.4778	340	Trillium Compact	200	5/9/2014
KAN14	GS	36.9568	-97.9630	363	Trillium Compact	200	8/20/2014
OK029	GS	35.7966	-97.4549	333	Trillium Compact	100	2/13/2014
OK032	GS	36.8038	-98.2104	345	Trillium Compact	100	3/4/2015
OK035	GS	36.7082	-98.7097	485	Trillium Compact	100	12/18/2015
OK916	NQ	36.8073	-97.7477	332	AC-63	200	12/21/2015
OK917	NQ	36.7586	-98.3574	363	AC-63	200	12/22/2015

Table 3. HypoDD parameters used for earthquake relocations.

Iteration	WTCTP	WTCTS	WRCT	WDCT	DAMP
1-3	1	0.7	-999	-999	150
4-8	1	0.7	4	3	100
9-13	1	0.9	2	1	80

Table 4. HASH parameters

Parameter	Value	Description
npolmin	7	Minimum number of polarities per event
dang	5°	Grid search angle
nmc	30	Number of trials
maxout	300	Maximum focal mechanism outputs
ratmin	3	Minimum allowed SNR
badfrac	0	Fraction of polarities assumed bad

qbadfac	0.3	Assumed noise in amplitude ratios
delmax	150 km	Maximum allowed epicentral distance
cangle	45°	Angle for computing mechanism probability
prob_max	0.1	Probability threshold for multiples

Table 5. Injection wells in NW area.

API	Latitude	Longitude	Monthly Rate	Cumulative Volume 2011-2015	Year	Month
3505322904	36.601487	-97.71438	250188	12009039	2012	June
3504724516	36.55634	-97.61396	218251	10476024	2012	Jan
3505323011	36.607885	-97.767041	134983	6479196	2012	Sept
3505300208	36.644972	-97.52425	129301	7758066	2006	Nov
3504724879	36.5784	-97.655269	103364	1240369	2015	Feb
3507124714	36.66744	-97.61753	77484	1859622	2014	Mar
3505323322	36.606486	-97.623189	63545	1525076	2014	Feb
3505322771	36.623055	-97.719527	55853	2680956	2012	Jan
3505322665	36.666677	-97.65803	41811	1505187	2013	Jan
3505323102	36.66486	-97.65803	22341	670243	2013	Apr
3505301035	36.672153	-97.68958	21386	1283160	1985	June
3505320785	36.686792	-97.505784	19167	230000	1981	Nov
3505301076	36.682771	-97.52961	18662	1119735	1959	Apr
3504724339	36.572688	-97.672612	14316	858983	2003	Feb
3505320937	36.623255	-97.75268	7777	466623	1982	May
3505321280	36.642281	-97.73353	7730	463810	1983	Sept
3505300943	36.597653	-97.55441	7143	428576	1993	Oct
3505301041	36.674009	-97.76393	4702	344397	1971	Dec
3505320030	36.678332	-97.729638	4049	48588	1966	Nov
3504722466	36.562789	-97.70021	3829	229720	1993	Dec
3505320044	36.613179	-97.63887	3441	206430	1996	Mar
3505322948	36.634025	-97.757766	3402	163270	2012	Apr
3504721538	36.551519	-97.73546	3115	37381	1984	Sept
3505320995	36.667649	-97.72001	2319	55650	2014	Apr
3505320136	36.672169	-97.70311	2264	27162	2015	Jan
3505320135	36.672169	-97.69861	2040	110689	1970	June
3504700780	36.583637	-97.70134	1700	102016	1987	June

3505320134	36.671262	-97.71098	1380	94406	1970	June
3505321286	36.605904	-97.61185	305	18326	1989	July

Table 6. Injection wells in SE area.

API	Latitude	Longitude	Monthly rate	Cumulative volume 2011-2015	Year	Month
3510322789	36.355632	-97.40923	1778	96600	2011	Aug
3510301882	36.356238	-97.408814	1700	11900	2011	Jan
3510321493	36.355654	-97.40587	15886	953170	2001	Aug
3510323259	36.458511	-97.364212	3819	91650	2014	Jan
3510323247	36.45993	-97.36219	3333	80000	1993	Oct
3510322613	36.440466	-97.361954	3111	149324	2012	Mar
3510324166	36.52003	-97.35972	45000	1080000	2014	Jan
3510321270	36.44846	-97.35546	519	62220	1987	Aug
3510301840	36.352043	-97.355143	2843	170556	1963	Oct
3510320750	36.324889	-97.3465	0	0	1996	July
3510323073	36.321348	-97.344115	3257	195405	1996	July
3510322811	36.527478	-97.321609	4471	53650	1987	Mar
3510323272	36.531118	-97.31573	3799	227945	2006	June
3510323195	36.542455	-97.29949	3609	173225	2012	Jan
3510320701	36.384741	-97.29273	5663	339755	1994	Sept
3510324178	36.555761	-97.290555	73026	4381575	2008	Nov
3510324448	36.404918	-97.290118	174913	8395842	2013	Feb
3510322346	36.382022	-97.28937	5694	341658	1988	June
3510320746	36.387913	-97.28657	7885	473120	1988	June
3510322341	36.385647	-97.28488	920	55182	1988	June
3510322912	36.378396	-97.28488	2940	176378	1989	Oct
3510301309	36.426142	-97.283531	3266	195970	1981	May
3510320700	36.382931	-97.28153	6014	360846	1989	Oct
3510320711	36.37568	-97.28153	0	0	1989	Oct
3510324375	36.46292	-97.27631	9842	472396	2012	Sept
3510322776	36.523426	-97.26139	5051	303081	1986	Sept
3510323430	36.493515	-97.26139	18278	1096680	2008	June
3510300240	36.464282	-97.26113	353	21156	2006	July
3510322387	36.323111	-97.24791	3900	233996	1997	Jan
3510324317	36.54628	-97.24575	74519	3576896	2013	July
3510320194	36.529769	-97.24571	2187	131204	1987	Dec
3510330021	36.546085	-97.24459	2164	129818	1994	Apr
3510322668	36.320389	-97.24455	3337	200239	1996	Dec
3510322431	36.333985	-97.24343	927	55609	1986	Sept

3510322309	36.326736	-97.243094	4705	56455	1997	Jan
3510322334	36.321296	-97.24007	3740	224373	1996	Dec
3510323365	36.324468	-97.23839	23644	567453	2014	June
3510324300	36.362417	-97.23713	153373	7361925	2012	Jan
3510322425	36.333986	-97.23559	1667	100003	2003	Jan
3510324539	36.35007	-97.22224	453913	11946425	2013	Dec
3510322572	36.506199	-97.22105	5711	342665	1985	June
3510320878	36.379286	-97.18967	833	39996	2009	July
3510324488	36.40509	-97.18636	36926	1329317	2013	June

Table 7. Injection wells in central uplift area.

API	Latitude	Longitude	Monthly rate	Cumulative volume 2011-2015	Year	Month
3504724630	36.54888	-97.46724	162534	7801636	2013	Mar
3510324364	36.577794	-97.424957	118034	5665630	2012	Oct
3510324286	36.59325	-97.382278	88329	4239773	2012	Jan
3510324351	36.5929	-97.38219	71523	3433089	2012	July
3510323298	36.564582	-97.39468	27208	1305960	1995	July
3510324026	36.56325	-97.43407	8100	486000	2006	Nov
3510301941	36.559617	-97.3835	5863	281400	1963	Aug
3510321151	36.544208	-97.38462	3375	162000	1997	Mar
3510301944	36.551459	-97.38687	2094	100500	1960	Nov
3510301051	36.566282	-97.347545	1948	116875	1981	Sept

Table 8. Injection wells in south-central uplift area.

API	Latitude	Longitude	Monthly rate	Cumulative volume 2011-2015	Year	Month
3504724761	36.2593	-97.5498	287195	3446343	2014	July
3504724620	36.27506	-97.46158	134970	4062242	2013	Aug
3504724848	36.319858	-97.477984	83629	2007106	2014	Oct
3504724729	36.317796	-97.552895	11888	285313	2014	Mar
3504724818	36.275787	-97.515708	11470	275277	2014	Sept
3504724668	36.21854	-97.48066	9849	266559	2013	Aug
3510302216	36.248621	-97.46074	5249	314962	1954	Feb
3510322943	36.298928	-97.45684	1259	75514	1990	Sept
3504701014	36.318736	-97.53328	542	32490	1956	Feb
3504700984	36.325905	-97.51087	19	1130	1967	Apr